THE JOURNAL OF PHYSICAL CHEMISTRY C

Article

pubs.acs.org/JPCC

# Vibrational Properties of CuO and $Cu_4O_3$ from First-Principles Calculations, and Raman and Infrared Spectroscopy

L. Debbichi,[†] M. C. Marco de Lucas,[†] J. F. Pierson,[‡] and P. Krüger*,[†]

[†]Laboratoire Interdisciplinaire Carnot de Bourgogne, UMR 6303 CNRS-Université de Bourgogne, F-21078 Dijon, France

[‡]Institut Jean Lamour, UMR CNRS 7198, Département CP2S, Ecole des Mines, F-54042 Nancy Cedex, France

Supporting Information

**ABSTRACT:** A combined experimental and theoretical study is reported on the vibrational properties of tenorite CuO and paramelaconite $Cu_4O_3$. The optically active modes have been measured by Raman scattering and infrared absorption spectroscopy. First-principles calculations have been carried out with the LDA+U approach to account for strong electron correlation in the copper oxides. The vibrational properties have been computed ab initio using the so-called direct method. Excellent agreement is found between the measured Raman and infrared peak positions and the calculated phonon frequencies at the Brillouin zone center, which allows the assignment of all prominent peaks of the $Cu_4O_3$ spectra. Through a detailed analysis of the displacement eigenvectors, it is shown that a close relationship exists between the Raman modes of CuO and $Cu_4O_3$.

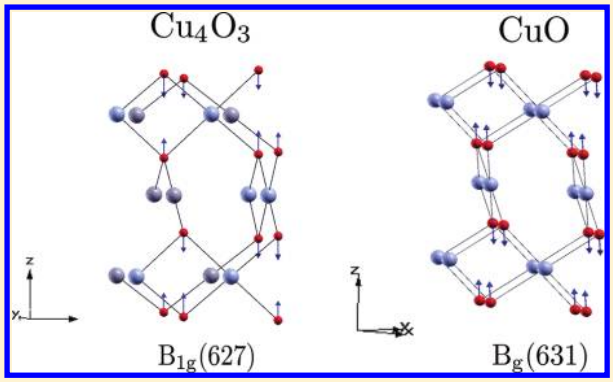


## INTRODUCTION

Copper oxide is a fascinating class of inorganic solids that has been the subject of intensive research for the past two decades. It has aroused considerable interest for multiple applications, including spintronic devices,[1−3] optoelectronic,[4] and photocatalysis.[5,6] In particular, the two main copper oxide phases, which are cupric (CuO) and cuprous ($Cu_2O$) oxide, are considered among the most important semiconductors with a band gap $E_g$ in the range of 1.7−2.2 eV.[7−9] $Cu_2O$ is a Bloch semiconductor, while CuO is usually regarded as a Mott or charge-transfer insulator driven by strong electron correlation. Because copper oxides are at the basis of most high-$T_c$ superconductors, it is important to understand their electronic and vibrational properties. Furthermore, both $Cu_2O$ and CuO appear as ideal oxygen carriers for chemical looping combustion applications,[10] and they have also been used as gas sensors[11] in solar energy conversion[12,13] and catalysis.[14−17] The lattice dynamics of $Cu_2O$ and CuO has been studied experimentally by infrared (IR) and Raman spectroscopy, exciton luminescence, and inelastic neutron scattering.[18−24] From the theoretical side, first-principles calculations have been reported for $Cu_2O$, while for CuO only semiempirical schemes were used.[21] These studies helped to gain understanding of the nature of the electron phonon interaction and the negative thermal expansion (NTE) in $Cu_2O$.[19,25] They provided information about the spin−phonon interaction[26,27] and the size-dependent electron−phonon coupling in CuO.[28]

In addition to cupric and cuprous oxide, an interesting intermediate phase, paramelaconite $Cu_4O_3$, was found in 1890 in specimens from the Copper Queen mine, Arizona.[29] Thin films of pure $Cu_4O_3$ have recently been obtained by reactive magnetron sputtering.[30] In $Cu_4O_3$, which may be written as $Cu_2^+Cu_2^{2+}O_3$, copper is present in both oxidation states Cu(I) and Cu(II). Therefore, also paramelaconite has potential applications in catalysis, for example, for low temperature conversion of organic contaminants present in air stream.[31]

Despite its importance, many properties of paramelaconite $Cu_3O_4$ are poorly understood, and its lattice dynamics have, to the best of our knowledge, not been investigated yet. In this Article, we report a combined experimental and theoretical study on the vibrational properties of the copper oxides phases CuO and $Cu_4O_3$. The structural parameters and zone-center phonons have been calculated from first principles using the local density approximation with Hubbard-U correction (LDA +U) to account for strong electron correlation. The calculated frequencies are compared to experimental infrared and Raman spectra, and all prominent peaks could be assigned for both $Cu_4O_3$ and CuO.

## EXPERIMENTAL DETAILS

Copper oxide films were deposited on glass and silicon substrates by magnetron sputtering of copper target (50 mm diameter, 3 mm thick, and purity higher than 99.9%) in Ar−$O_2$ reactive mixture. The experimental device is a 40 L sputtering chamber pumped down via a mechanical pump and a turbomolecular pump, allowing a base vacuum of $10^{-4}$ Pa.

**Received:** March 31, 2012
**Revised:** April 18, 2012
**Published:** April 18, 2012

   dx.doi.org/10.1021/jp303096m | J. Phys. Chem. C 2012, 116, 10232−10237

The films were deposited without external heating, and the deposition temperature was close to 50 °C. Further details on the deposition reactor, substrate cleaning, and deposition procedure have been reported previously.[30] Moreover, pure CuO films were also obtained by air annealing of paramelaconite films up to 400 °C.[32] The crystal structures were checked by X-ray diffraction. $Cu_2O$, CuO, and $Cu_4O_3$ films about 200 nm thick grown on glass substrates were used for the micro-Raman analyses, while a 500 nm thick paramelaconite $Cu_4O_3$ film deposited on a Si substrate was used for IR absorption measurements.

Raman spectra were obtained with a HORIBA T64000 spectrometer equipped with a confocal microscope and a nitrogen-cooled CCD detector. The spectra were recorded in a backscattering configuration. The excitation was provided by an Spectra-Physics Stabilite 2018 Ar−Kr laser. The excitation line was at 514 nm, and the laser power was kept low enough to avoid heating of the samples. Transmission IR spectra were obtained with a BRUKER Vertex 70v spectrometer.

## COMPUTATIONAL DETAILS

Calculations were performed within the framework of density functional theory (DFT) using the VASP package.[33−35] The projector-augmented-wave (PAW) method was employed with 6 and 11 valence electrons for oxygen and copper atoms, respectively. The plane-wave cutoff was 600 eV.[36] As exchange-correlation function, the local spin density approximation (LSDA), was used, together with the "LDA+U" correction for the on-site Coulomb interaction of Cu-3d states.[37] The structures were relaxed to equilibrium geometry using the RMM-DIIS algorithm to achieve cell stress and atomic force convergence.[38] The self-consistent electronic loop was stopped when the total (free) energy change was smaller than $10^{-8}$ eV. The ionic positions and the lattice constants were optimized until the forces acting on each atom were less than $10^{-6}$ eV/Å. The vibrational properties were determined by the direct method,[39] with forces calculated ab initio via the Hellmann−Feynman theorem. The forces were computed for independent displacements required by the symmetry of the unit cell. The displacement amplitudes were 0.03 Å. Positive and negative atomic displacements along *x*, *y*, and *z* directions were used for all of the structures. With the chosen numerical settings, high structural accuracy was achieved, ensuring stable results for vibrational quantities.

## RESULTS AND DISCUSSION

**Structural Optimization.** We start with a short description of the crystal structures of the considered phases. CuO tenorite has monoclinic symmetry with space group $C2/c$;[40,41] see Figure 1. There are four Cu−O molecules in the unit cell, and two Cu−O units in the primitive cell. The copper and oxygen sites have $C_i$ and $C_2$ symmetry, respectively. Each copper atom is located in the center of an oxygen parallelogram. Each oxygen atom, in turn, has a distorted tetrahedral copper coordination. Paramelaconite $Cu_4O_3$ crystallizes in the tetragonal space group $I4_1/amd$[42] with four inequivalent sites (see Table 1) and four formula units in the tetragonal cell ($Cu_{16}O_{12}$); see Figure 1. $Cu_4O_3$ is an intermediate compound between CuO and $Cu_2O$ and contains an equal number of magnetic Cu(II) and magnetically inert Cu(I) ions. It consists of chains of edge-sharing, square-planar $CuO_4$ units, as in CuO, and zigzag chains of $CuO_2$ units with linearly coordinated Cu(I) ions, as in $Cu_2O$. The orientation of both chain types alternates between the *a* and *b* crystal axes.

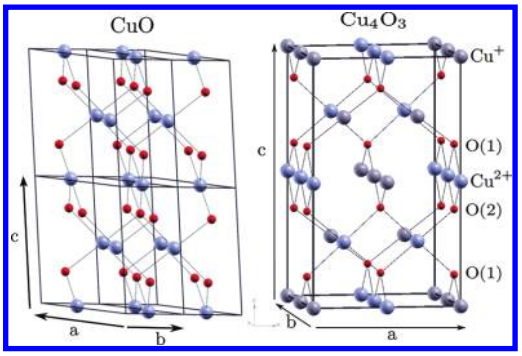


**Figure 1.** Ball-and-stick model of the tenorite CuO (left) and the paramelaconite $Cu_4O_3$ (right). O in red, $Cu^{2+}$ in blue, and $Cu^+$ in gray.

**Table 1. Reduced Atomic Coordinates and Wyckoff Symbols of Paramelaconite $Cu_4O_3$**

| atom | Wyckoff | *x* | *y* | *z* |
|---|---|---|---|---|
| Cu(1) | 8(c) | 0 | 0 | 0 |
| Cu(2) | 8(d) | 0 | 0 | 1/2 |
| O(1) | 8(e) | 0 | 1/4 | *z* |
| O(2) | 4(a) | 0 | 1/4 | 3/8 |

Both CuO and $Cu_4O_3$ have antiferromagnetic insulating ground states, but the local spin-density approximation (LSDA) to DFT describes them as paramagnetic metals.[43] To correct this shortcoming of the LSDA, electron correlation has herein been taken into account in the LDA+U approach. For the Cu-3d Coulomb integral *U* and the exchange integral *J*, generally accepted parameter values for CuO, $U = 7.5$ eV, $J = 0.98$ eV[43] have been used. The lattice structures were fully optimized in the proper magnetic supercell. The optimized structural parameters, listed in Table 2, agree well with experiment. For CuO, the lattice constants *a*,*b*,*c* are slightly underestimated by 2.9%, 3.4%, and 4.4%, respectively. For $Cu_4O_3$, the error is 2.4% for *a* and 1.8% for *c*. Note that the LDA+U correction is needed not only for the correct electronic ground state, but also for obtaining equilibrium structures in agreement with experiment. This is a crucial requirement for a good description of the vibrational properties.

**Table 2. Lattice Parameters and Internal Coordinates [*y*(*b*) and *z*(*c*)] of CuO and $Cu_4O_3$**

| system | parameter | calculation (this work) | experiment |
|---|---|---|---|
| CuO | *a* (Å) | 4.548 | 4.684,[40] 4.653[41] |
| | *b* (Å) | 3.305 | 3.423,[40] 3.410[41] |
| | *c* (Å) | 4.903 | 5.129,[40] 5.108[41] |
| | *β* (deg) | 99.652 | 99.54,[40] 99.483[41] |
| | *y* (*b*) | 0.4137 | 0.416[40] |
| $Cu_4O_3$ | *a* (Å) | 5.595 | 5.873,[42] 5.817[29] |
| | *c* (Å) | 9.650 | 9.932,[42] 9.861[29] |
| | *z* (*c*) | 0.115 | 0.12[42] |

**Phonon Spectra.** Figure 2 shows the experimental Raman spectra of CuO and $Cu_4O_3$ along with that of $Cu_2O$ for comparison. The CuO and $Cu_2O$ spectra agree well with the literature.[22,23,27] Although the $Cu_4O_3$ phase is a chemical and structural intermediate of CuO and $Cu_2O$, its Raman spectrum


dx.doi.org/10.1021/jp303096m | J. Phys. Chem. C 2012, 116, 10232−10237

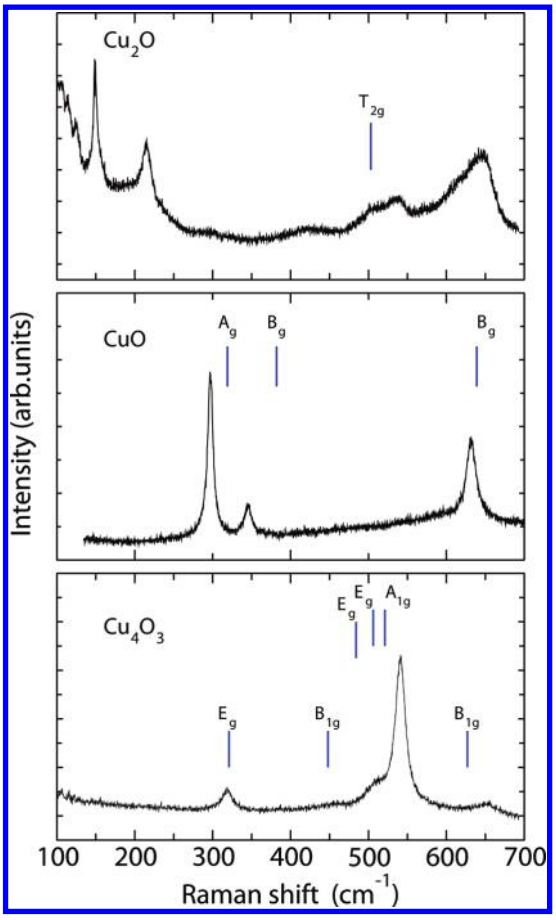


**Figure 2.** Experimental Raman spectra of $Cu_2O$, CuO, and $Cu_4O_3$. The calculated frequencies of Raman active vibrational modes are indicated by vertical bars.

looks completely different and can thus be a very useful probe for phase analysis.

The vibrational properties of CuO have been analyzed before using group theory and semiempirical calculations.[21] CuO has 12 phonon branches because there are four atoms in the primitive cell. A factor-group analysis gives the following zone-center modes:

$$\Gamma_{vibr} = A_g + 2B_g + 4A_u + 5B_u$$

The three acoustic modes are of $A_u + 2B_u$ symmetry. Among the nine optical modes, three $(A_g + 2B_g)$ are Raman-active, and the remaining six $(3A_u + 3B_u)$ are IR-active.[44] In the $A_g$ and $B_g$ Raman modes only the oxygen atoms move, with displacements in the *b*-direction for $A_g$ and perpendicular to the *b*-axis for $B_g$ modes. The infrared active modes involve the motion of both the O and the Cu atoms. The induced dipole moment is along the *b*-axis for the $A_u$ modes and perpendicular to it for the $B_u$ modes.

Here, the vibrational modes of the copper oxides were calculated ab initio using the direct method[39] from the theoretical equilibrium structures. Depending on crystal symmetry, 12 or 22 displacements were used in negative and positive direction for CuO and $Cu_4O_3$, respectively. In Tables 3 and 4, the calculated zone-center modes of CuO and $Cu_3O_4$ are listed and compared to the present Raman (Figure 2) and IR (Figure 3) experiments and to literature data. Because both CuO and $Cu_4O_3$ have inversion symmetry, Raman and IR

**Table 3. Calculated Frequencies $\omega_c$ of Zone-Center ($\Gamma$) Phonons for Tenorite CuO, As Compared to Experimental Values ($\omega_e$) in $cm^{-1}$[a]**

| sym | activity | $\omega_c$ | $\omega_e$ (this work) | $\omega_e$ (other) |
|---|---|---|---|---|
| $B_u$ | IR | 141 | | 147[21,24] |
| $A_u$ | IR | 164 | | 161[21,24] |
| $A_g$ | Raman | 319 | 296 | 301−303[27,44] |
| $A_u$ | IR | 327 | | 321[21,24] |
| $B_g$ | Raman | 382 | 346 | 348−350[27,44] |
| $A_u$ | IR | 457 | | 478[21,24] |
| $B_u$ | IR | 503 | | 533[21,24] |
| $B_u$ | IR | 568 | | 587[21,24] |
| $B_g$ | Raman | 639 | 631 | 633−636[27,44] |

[a]Symmetries (sym) and Raman or infrared activity are indicated.

**Table 4. Calculated ($\omega_c$) and Measured ($\omega_e$) Frequencies (in $cm^{-1}$) of the Zone-Center Modes of $Cu_4O_3$**

| Raman | | | IR | | | silent | |
|---|---|---|---|---|---|---|---|
| sym | $\omega_c$ | $\omega_e$ | sym | $\omega_c$ | $\omega_e$ | sym | $\omega_c$ |
| $E_g$ | 321 | 318 | $E_u$ | 50 | | $B_{2u}$ | 59 |
| $B_{1g}$ | 448 | | $E_u$ | 99 | | $B_{1u}$ | 104 |
| $E_g$ | 484 | | $E_u$ | 121 | | $A_{1u}$ | 107 |
| $E_g$ | 506 | 510 | $A_{2u}$ | 127 | | $B_{1u}$ | 130 |
| $A_{1g}$ | 521 | 541 | $E_u$ | 168 | 164 | $A_{1u}$ | 154 |
| $B_{1g}$ | 627 | 651 | $E_u$ | 214 | 212 | $B_{2u}$ | 160 |
| | | | $A_{2u}$ | 224 | | $B_{2u}$ | 305 |
| | | | $A_{2u}$ | 309 | 322 | $B_{2u}$ | 348 |
| | | | $E_u$ | 454 | 463 | $B_{2u}$ | 603 |
| | | | $E_u$ | 538 | 548 | | |
| | | | $A_{2u}$ | 576 | | | |
| | | | $E_u$ | 603 | 607 | | |
| | | | $A_{2u}$ | 649 | | | |

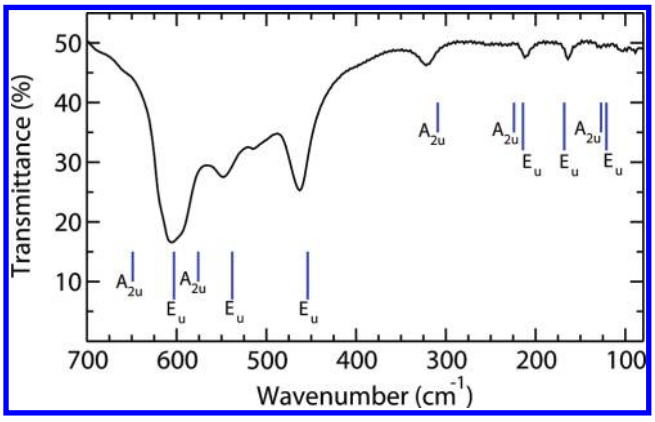


**Figure 3.** Experimental infrared absorption spectrum of $Cu_4O_3$ measured in transmittance. The calculated frequencies of infrared active vibrational modes are indicated by vertical bars.

active modes do not mix. The present ab initio results on CuO agree very well both with experiment (Figure 2) and previous semiempirical calculations (Table 2). We have also calculated the structural and vibrational properties of cuprite $Cu_2O$. According to the group theoretical selection rules, the cuprite structure allows only a single Raman-active mode ($T_{2g}$). Its calculated frequency is indicated in Figure 2 and corresponds to the broad feature seen in experiment at $\omega \approx 500-550$ $cm^{-1}$. For further details, including a discussion of the additional


dx.doi.org/10.1021/jp303096m | J. Phys. Chem. C 2012, 116, 10232−10237

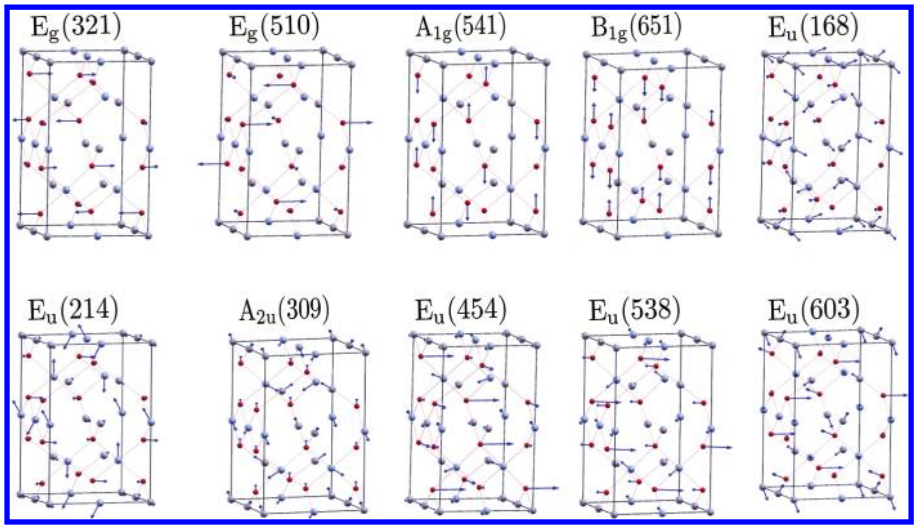


**Figure 4.** Calculated vibrational modes of $Cu_4O_3$ labeled by symmetry and frequency given in parentheses in $cm^{-1}$. The atomic displacements are shown by arrows in log 10 scale.

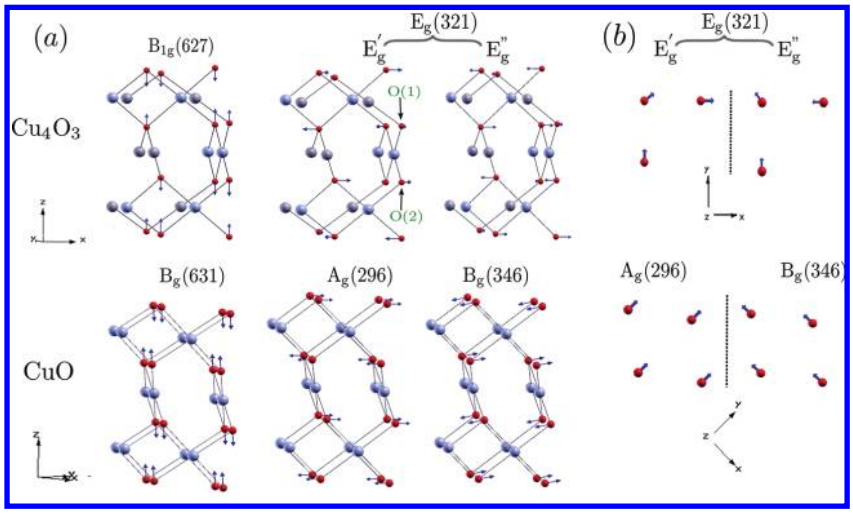


**Figure 5.** Comparison between calculated Raman modes of CuO and $Cu_4O_3$. (a) $E_g'$ and $E_g''$ are a particular choice of eigenvectors of the 2-fold mode $E_g(321)$. (b) Top view of the topmost oxygen layer.

peaks observed in the $Cu_2O$ Raman spectrum, see the Supporting Information.

Now we turn to the vibrational properties of $Cu_4O_3$ for which we are not aware of any works in the literature. For the paramelaconite structure, group theory predicts 42 vibrational modes with the following irreducible representations at the Γ-point of the Brillouin zone:

$$\Gamma_{vibr} = 3E_g + A_{1g} + 2B_{1g} + 9E_u + 6A_{2u} + 5B_{2u} + 2B_{1u} + 2A_{1u}$$

$A_{2u} + E_u$ are the acoustic modes. All others are optical modes, among which nine are Raman active ($A_{1g}$, $B_{1g}$, and $E_g$), 21 are IR active ($A_{2u}$ and $E_u$), and nine are silent ($A_{1u}$, $B_{1u}$, and $B_{2u}$). In the Raman spectrum (Figure 2), four peaks are clearly observed, which can all be assigned to particular vibrational modes through comparison with the calculated frequencies; see Table 4. The most intense Raman line at 541 $cm^{-1}$ corresponds to an $A_{1g}$ mode, while the weaker peaks at 318, 510, and 651 $cm^{-1}$ correspond to $E_g$, $E_g$, and $B_{1g}$ modes, respectively. Likewise, the six most prominent peaks of the IR spectrum (Figure 3) could be assigned to IR-active modes; see Table 4. Among them, five are of $E_u$ and one is of $A_{2u}$ symmetry. While all of the calculated $E_u$ modes above 150 $cm^{-1}$ are observed as distinct peaks in the experimental spectrum, most $A_{2u}$ modes are not, probably due to low intensity. Note, however, that the weak shoulder structures on the left and right sides of the dominating $E_u$ peak at 603 $cm^{-1}$ roughly coincide with two $A_{2u}$ frequencies; see Figure 3.

For all experimentally observed modes, the atomic displacement vectors are shown in Figure 4. In the Raman active gerade modes, only the O atoms move. For the one-dimensional modes $A_{1g}$ and $B_{1g}$, the O motion is along the crystal axis *c*, while in the two-dimensional modes ($E_g$), the O atoms move in the *ab* plane. In the $A_{1g}$ mode, which dominates the Raman spectrum, only the O(1) atoms oscillate along the 2-fold axis of the tetrahedron formed by two $Cu^{2+}$ and two $Cu^{+}$ neighbors of O(1). Note that this is the only possible motion for the fully symmetrical mode ($A_{1g}$) because the *z*-coordinate of O(1) is the only internal structural parameter. Similarly, in CuO, where the only internal parameter is the *y*-coordinate of the O site, the strongest Raman peak corresponds to the fully symmetrical $A_g$


dx.doi.org/10.1021/jp303096m | J. Phys. Chem. C 2012, 116, 10232−10237

mode where the O atoms move along *b*. The large intensity of the $A_{1g}$ mode in $Cu_4O_3$ is related to the fact that the moving O(1) atom is located at a low symmetry site and the mode involves the asymmetric stretching of inequivalent Cu−O bonds (see the Supporting Information for details). In the $B_{1g}$ mode, all O atoms move along *c* with comparable amplitude such that the width of the square-planar $CuO_4$ chains oscillates. In the $E_g$ modes, all O atoms move in the *ab* plane. In the $E_g(510)$ mode, the O(1) atoms move perpendicular to the $CuO_4$ chains that they are part of, and the O(2) displacement has a much smaller amplitude. In the $E_g(321)$ mode, all O atoms vibrate with comparable amplitude.

The paramelaconite and tenorite structures are closely related. $Cu_4O_3$ can be viewed as a CuO crystal without monoclinic distortion and where one-fourth of the oxygen atoms has been removed.[45−47] As a consequence, a strong link exists between the vibrational properties of the two structures as we shall now show for the Raman modes. When lowering the point symmetry from the $D_{4h}$ to $C_{2h}$, $B_{1g}$ evolves to $B_g$ and $E_g$ splits into $A_g$ and $B_g$ modes. As seen in Figure 2 and Table 4, the $Cu_4O_3$ peak at $\omega_c$ = 627 $cm^{-1}$ ($B_{1g}$) is very close to the CuO peak at $\omega_c$ = 631 $cm^{-1}$ ($B_g$). The corresponding vibrational modes are almost the same, see Figure 5. The only difference is that in CuO the displacement vectors have a small *x*-component due to the monoclinic distortion of the lattice. Also, for the other two CuO modes, at $\omega_c$ = 296 $cm^{-1}$ ($A_g$) and $\omega_c$ = 346 $cm^{-1}$ ($B_g$), the frequencies are close to those of the double degenerate $E_g$ mode of $Cu_4O_3$ at $\omega_c$ = 321 $cm^{-1}$. In the CuO modes, the O atoms vibrate along the *b* axis for $A_g(296)$, and approximately along *a* in $B_g(246)$. Also, for the $Cu_4O_3$ mode $E_g(321)$, all O atoms are displaced in the *xy* plane. Figure 5 shows a set of two orthogonal eigenmodes ($E_g'$, $E_g''$) of the $Cu_4O_3$-$E_g(321)$ manifold. $E_g'$ has been chosen such that its O(2) displacement vector is aligned with that of CuO-$A_g(296)$. The O(1) vectors are turned away from those of O(2) by about ±45°. Nevertheless, the total vibrational modes $E_g'$ and $A_g$ are very similar. The same observations hold for the modes $Cu_4O_3$-$E_g''$ and CuO-$B_g(346)$. This comparison clearly shows that the $Cu_4O_3$ mode $B_{1g}(627)$ corresponds to the CuO mode $B_g(631)$, and that $Cu_4O_3$ mode $E_g(321)$ is split into the CuO modes $A_g(296)$ and $B_g(346)$.

While the Cu atoms are immobile in the Raman-active gerade modes, they show small but nonzero displacements in the IR-active ungerade modes. The O atoms move along the *c* axis in the $A_{2u}$ mode, and perpendicular to it in the $E_u$ mode. The most intense IR-active mode, $E_u(603)$, is a sort of bending mode of the square-planar $CuO_4$ units, where the O(1) has maximum displacement perpendicular to the $CuO_4$ plane. Substantial amplitude is also found on the Cu(1) atoms, and the mode appears as an asymmetric stretching of the $CuO_2$ zigzag chains. The second strongest IR peak, $E_u(454)$, also appears like a bending mode, within both the $CuO_4$ and the $CuO_2$ chains. Here, the O(1) atoms show large displacements along the $CuO_4$ chains.

## SUMMARY AND CONCLUSIONS

We have presented an experimental and theoretical investigation of the vibrational properties of the copper oxides CuO and $Cu_4O_3$. The Raman and infrared spectra of parmamelaconite $Cu_4O_3$ were measured for the first time. They are very different from those of CuO and $Cu_2O$, and may thus serve as fingerprints in structural analyses. The structural and vibrational properties of the tenorite and paramelaconite copper oxide phases were calculated from first principles, and good agreement with experiment was obtained in all cases. The peak assigmnent of the CuO Raman spectrum, which had previously relied on semiempirical modeling, has herein been confirmed by ab initio calculations. All prominent peaks of the Raman and infrared spectra of $Cu_4O_3$ coincide with calculated frequencies and could thus be assigned to the normal modes of the paramelaconite crystal. By comparison of the calculated displacement vectors, it has been shown explicitly that several $Cu_4O_3$ Raman modes directly derive from CuO.

## ASSOCIATED CONTENT

### Supporting Information

Additional calculations on cuprous oxide $Cu_2O$ are reported for comparison. Furthermore, a qualitative explanation is given for the large intensity of the $A_{1g}$ peak in the $Cu_4O_3$ Raman spectrum. This material is available free of charge via the Internet at http://pubs.acs.org.

## AUTHOR INFORMATION

### Corresponding Author

*E-mail: pkruger@u-bourgogne.fr.

### Notes

The authors declare no competing financial interest.

## ACKNOWLEDGMENTS

We acknowledge funding from the Région Bourgogne through the PARI-STM9 grant and computing time provided by GENCI-CINES and by the Centre de Ressources Informatiques of the Université de Bourgogne. We thank Dr. Lucien Saviot for stimulating discussions and a careful reading of this manuscript.

## REFERENCES

(1) Wei, M.; Braddon, N.; Zhi, D.; Midgley, P. A.; Chen, S. K.; Blamire, M. G.; MacManus-Driscoll, J. L. *Appl. Phys. Lett.* **2005**, *86*, 072514−072517.
(2) Sieberer, M.; Redinger, J.; Mohn, P. *Phys. Rev. B* **2007**, *75*, 035203−035210.
(3) Yang, S. G.; Li, T.; Gu, B. X.; Du, Y. W.; Sung, H. Y.; Hung, S. T.; Wong, C. Y.; Pakhomov, A. B. *Appl. Phys. Lett.* **2003**, *83*, 3746−3749.
(4) Yanagi, H.; Inoue, S.; Ueda, K.; Kawazoe, H.; Hosono, H.; Hamada, N. *J. Appl. Phys.* **2000**, *88*, 4159−4164.
(5) Akimoto, K.; Ishizuka, S.; Yanagita, M.; Nawa, Y.; Paul, G. K.; Sakurai, T. *Sol. Energy* **2006**, *80*, 715−722.
(6) Liu, Y.; Turley, H. K.; Tumbleston, J. R.; Samulski, E. T.; Lopez, R. *Appl. Phys. Lett.* **2011**, *98*, 162105−162108.
(7) Marabelli, F.; Parravicini, G. B.; Salghetti-Drioli, F. *Phys. Rev. B* **1995**, *52*, 1433−1436.
(8) Hu, J. P.; Payne, D. J.; Egdell, R. G.; Glans, P.-A.; Learmonth, T.; Smith, K. E.; Guo, J.; Harrison, N. M. *Phys. Rev. B* **2008**, *77*, 155115−155125.
(9) Nikitine, S.; Grun, J. B.; Sieskind, M. *J. Phys. Chem. Solids* **1961**, *17*, 292−300.
(10) Goldstein, E. A.; Mitchell, R. E. *Proc. Combust. Inst.* **2011**, *33*, 2803−2810.
(11) Poizot, P.; Laruelle, S.; Grugeon, S.; Taracon, J. M. *Nature (London)* **2000**, *407*, 496−499.
(12) Wang, M.; Xie, F.; Xie, W.; Zheng, S.; Ke, N.; Chen, J.; Zhao, N.; Xu, J. B. *Appl. Phys. Lett.* **2011**, *98*, 183304−183307.
(13) Ray, S. C. *Sol. Energy Mater. Sol. Cells* **2001**, *68*, 307−312.
(14) Li, J. L.; Takeguchi, T.; Inui, T. *Appl. Catal., A* **1996**, *139*, 97−106.
(15) Ishihara, T.; Higuchi, M.; Takagi, T.; Ito, M.; Nishiguchi, H.; Takita, T. *J. Mater. Chem.* **1998**, *8*, 2037−2042.

(16) Pike, J.; Chan, S.-W.; Zhang, F.; Wang, X.; Hanson, J. *Appl. Catal., A* **2006**, *303*, 273−277.
(17) Marion, M. C.; Garbowski, E.; Primet, M. *J. Chem. Soc., Faraday Trans.* **1991**, *87*, 1795−1800.
(18) Beg, M. M.; Shapiro, S. M. *Phys. Rev. B* **1976**, *13*, 1728−1734.
(19) Mittal, R.; Chaplot, S. L.; Mishra, S. K.; Bose, P. P. *Phys. Rev. B* **2007**, *75*, 174303−174311.
(20) Yu, P. Y.; Shen, Y. R. *Phys. Rev. Lett.* **1974**, *32*, 373−376.
(21) Reichardt, W.; Gompf, F.; Aïn, M.; Wanklyn, B. M. *Z. Phys. B* **1990**, *81*, 19−24.
(22) Petroff, Y.; Yu, P. Y.; Shen, Y. R. *Phys. Rev. B* **1975**, *12*, 2488−2495 and references therein.
(23) Ivanda, M.; Waasmaier, D.; Endriss, A.; Ihringer, J.; Kirfel, A.; Kiefer, W. *J. Raman Spectrosc.* **1997**, *28*, 487−493 and references therein.
(24) Dar, M. A.; Ahsanulhaq, Q.; Kim, Y. S.; Sohn, J. M.; Kim, W. B.; Shin, H. S. *Appl. Surf. Sci.* **2009**, *255*, 6279−6284.
(25) Bohnen, K. P.; Heid, R.; Pintschovius, L.; Soon, A.; Stampfl, C. *Phys. Rev. B* **2009**, *80*, 134304−134310.
(26) Kuz'menko, A. B.; van der Marel, D.; van Bentum, P. J. M.; Tishchenko, E. A.; Presura, C.; Bush, A. A. *Phys. Rev. B* **2001**, *63*, 094303−094318.
(27) Chen, X. K.; Irwin, J. C.; Franck, J. P. *Phys. Rev. B* **1995**, *52*, 13130−13133.
(28) Fan, H.; Zou, B.; Liu, Y.; Xie, S. *Nanotechnology* **2006**, *17*, 1099−1103.
(29) Frondel, C. *Am. Mineral.* **1941**, *26*, 657−672.
(30) Pierson, J. F.; Thobor-Keck, A.; Billard, A. *Appl. Surf. Sci.* **2003**, *210*, 359−367.
(31) Medina-Valtierra, J.; Frausto-Reyes, C.; Camarillo-Martínez, G.; Ramírez-Ortiz, J. A. *Appl. Catal., A* **2009**, *356*, 36−42.
(32) Thobor, A.; Pierson, J. F. *Mater. Lett.* **2003**, *57*, 3676−3680.
(33) Kresse, G.; Joubert, D. *Phys. Rev. B* **1999**, *59*, 1758−1775.
(34) Kresse, G.; Hafner, J. *Phys. Rev. B* **1993**, *47*, 558−561.
(35) Kresse., G.; Hafner, J. *Phys. Rev. B* **1994**, *49*, 14251−14269.
(36) Blochl, P. E. *Phys. Rev. B* **1994**, *50*, 17953−17979.
(37) Dudarev, S. L.; Botton, G. A.; Savrasov, S. Y.; Humphreys, C. J.; Sutton, A. P. *Phys. Rev. B* **1998**, *57*, 1505−1509.
(38) Pulay, P. *Chem. Phys. Lett.* **1980**, *73*, 393−398.
(39) Parlinski, K.; Li, Z-.Q.; Kawazoe, Y. *Phys. Rev. Lett.* **1997**, *78*, 4063−4066.
(40) Åsbrink, S.; Norrby, L. J. *Acta Crystallogr., Sect. B* **1970**, *26*, 8−15.
(41) Wyckoff, R. W. G. *Crystal Structures*; Interscience Publishers: New York, 1963.
(42) O'Keeffe, M.; Bovin, J.-O. *Am. Mineral.* **1978**, *63*, 180−185.
(43) Wu, D.; Zhang, Q. *Phys. Rev. B* **2006**, *73*, 235206−235212.
(44) Kliche, G.; Popovic, Z. V. *Phys. Rev. B* **1990**, *42*, 10060−10066 and references therein.
(45) Pinsard-Gaudart, L.; Rodriguez-Carvajal, J.; Gukasov, A.; Monod, P. *Phys. Rev. B* **2004**, *69*, 104408−104417.
(46) Wang, X.; Hanson, J. C.; Frenkel, A. I.; Kim, J.; Rodriguez, J. A. *J. Phys. Chem. B* **2004**, *108*, 13667−13673.
(47) Kim, J. Y.; Rodriguez, J. A.; Hanson, J. C.; Frenkel, A. I.; Lee, P. L. *J. Am. Chem. Soc.* **2003**, *125*, 10684−10692.